J. Phys. D: Appl. Phys. **31** (1998) 1219–1232. Printed in the UK PII: S0022-3727(98)87965-5

Simulation of a decaying SF_6 arc plasma: hydrodynamic and kinetic coupling study

J-B Belhaouari, J-J Gonzalez and A Gleizes

Centre de Physique des Plasmas et de leurs Applications de Toulouse (CPAT), ESA du CNRS no 5002 Université Paul Sabatier, 118 route de Narbonne, 31062 Toulouse cedex 4, France

Received 29 September 1997, in final form 18 December 1997

Abstract. During the decay of a circuit-breaker arc, the plasma is subjected to strong blowing which can lead to deviations from chemical equilibrium. The intense convection may therefore be responsible for the presence of cold gas in the hot parts of the plasma. The cold particles then rapidly recombine with electrons, modifying the resistivity of the plasma. In order to study this phenomenon as it appears in circuit-breakers, we made a modelling of the extinction of an SF_6 arc for a simplified geometry. The two-dimensional model that was set up was followed by a study of the kinetics of SF_6 which enabled us to identify the various reaction processes governing the disappearance of electrons.

The results show that convection acts on S_2 molecules which, at the edge of the discharge and for temperatures of between 4000 and 6000 K, are overpopulated with respect to equilibrium. Through charge exchange processes between S_2 and S_2^+ particles, the overpopulation of S_2 leads to an overpopulation of the S_2^+ ions. These ions mainly recombine with electrons, lowering the electron population and modifying the electrical conductivity of the plasma.

Nomenclature

B_θ	magnetic field (T)
C_P	total specific heat at constant pressure (J K^{-1} kg^{-1})
Ca_i	number of i particles created by unit of time and volume (m^{-3} s^{-1})
Da_i	total destruction rate for i particles (s^{-1})
D	inlet flow (kg s^{-1})
d	mean length (m)
E_x	axial electric field (V m^{-1})
G	linear conductance (S)
h	enthalpy (J kg^{-1})
I	current intensity (A)
j_x	axial current density (A m^{-2})
k_b	Boltzmann's constant (J K^{-1})
K_d	direct reaction rate
K_i	reverse reaction rate
m_i	mass of species i (kg)
n_i	number density of species i (m^{-3})
P	pressure (Pa)
r	radial distance (m)
t	time (s)
T	temperature (K)
u	axial velocity (m s^{-1})
v	radial velocity (m s^{-1})
$\boldsymbol{V}$	vector velocity (m s^{-1})
x	axial distance (m)
Δt	time step (s)
ε_N	net emission coefficient (W m^{-3} sr^{-1})
κ	total thermal conductivity (W K^{-1} m^{-1})
μ	dynamic viscosity (kg m^{-1} s^{-1})
μ_0	vacuum permeability
ρ	mass density (kg m^{-3})
σ	electrical conductivity (S m^{-1})
τ^i	relaxation time of species i (s)

1. Introduction

The first physical models of SF_6 circuit-breaker arcs assumed local thermodynamic equilibrium (LTE). Two types of study were reported. The first concerned hydrodynamic studies, and originally these arc models were very simplified [1, 2], then simulations appeared which took laminar flow into account [3, 4]. To explain why SF_6 is more suitable than nitrogen, and using data from previous studies [5, 6], turbulence was included in these simplified geometry models of circuit-breaker arcs [7–9, 10]. Other models focused on studying decay in wall-stabilized arcs [11, 12]. In recent years, the models used have become increasingly sophisticated, dealing with both stationary states and decay and taking into account turbulence phenomena as well as more complex two-dimensional geometry [13–18].

The second type of study involved kinetics: the models developed in [19–24], for example, calculate the densities of the chemical species over time starting from a given initial composition and following a temperature decay law. However, this type of model is unable to study the influence of the injection of cold gas into the hot regions. Indeed, as the pressure is assumed to be constant and the model dimension less, the convection term is replaced by terms of particle input [19, 24, 25]. These substitution terms introduce particles of the same type as those already occurring in the plasma and do not take into account the fact that the gas actually sent into the plasma is cold SF_6 and that its dissociation is not instantaneous.

During extinction there is strong arc blowing leading to turbulence phenomena. The mechanisms involved are responsible for the energy transfer necessary for the recovery of dielectric rigidity. So a model based on thermal phenomena alone cannot explain the behaviour of the plasma where chemical non-equilibrium exists as a result of turbulence or strong cooling (-10^8 K s^{-1}). All the models based on the hypothesis of LTE lead to a post-arc current, unlike in experimental results where post-arc current is often non-existent after the zero of the alternating current. To interpret this difference, we have to consider that molecular species may be present in the hot regions. So, the plasma column could be cut by a portion of gas with low electrical conductivity hindering the circulation of electric current.

The general aim of this work is to simulate decaying arc behaviour taking non-equilibrium effects into account. The work does not aim to model exactly the behaviour of a circuit breaker or to represent the whole life cycle of the arc (creation, high current, decrease of the intensity, evolution near current zero, post arc phase and the dielectric phase), but to study the post-arc phase of the thermodynamic plasma without application of an RRRV (rate of rise of recovery voltage). So, we built a mathematical model which couples, in simplified geometry, a hydrodynamic and a kinetic study for SF_6 gas in a two-dimensional flow in a transient state at a pressure of 10^5 Pa. Coupling between hydrodynamics and kinetics is achieved through the pressure and the mass density.

The work is divided into three parts. The first (section 2) presents the SF_6 plasma composition in the stationary state. The second part (section 3) focuses on the study of SF_6 kinetics. Here, we study the species involved in the processes leading to electron disappearance and those that may be influenced by the strong convection brought about by arc decay. In the third part (section 4), we present the foundations of the hydrokinetic model such as the assumptions made, the geometry and the boundary conditions as well as all the equations that enable us to calculate the profiles of temperature, velocity and density over time; the results are then analysed considering the departures from equilibrium.

2. SF_6 plasma composition

2.1. Introduction

The calculation of the composition by a kinetics model has several aims:

Table 1. (*a*) Chemical reaction scheme.

No	Chemical reaction	Ref.
1	$F^+ + e + e \leftrightarrow F + e$ $F^+ + e \rightarrow F + h\nu$	[28]
2	$S^+ + e + e \leftrightarrow S + e$ $S^+ + e \rightarrow S + h\nu$	[28]

(i) It enables an indirect check to be made of the calculation of the direct and the reverse rates by comparing the composition obtained with the results in the literature obtained by another method. This stage therefore validates our subroutine for the calculation of microreversibility which is then used throughout arc decay.

(ii) The composition obtained is tabulated versus temperature and enables the stationary state density field to be set as an initial condition for the 2D model.

(iii) The equilibrium composition is used as a reference to study deviations from equilibrium during arc decay.

(iv) From the composition and the values of the reaction rates obtained in the stationary state we can estimate the reaction rates and the relaxation times of the various chemical reactions. These data are useful for interpretation as they indicate the most probable reactions over a given temperature range.

2.2. Hypothesis

Here, we present the assumptions made to calculate the composition using the kinetics model:

(i) The medium is homogeneous and in thermal equilibrium.

(ii) The energy distribution functions of all species are Maxwellian.

(iii) The reaction rates are solely determined by the mean stationary temperature.

(iv) There are no external forces.

(v) The pressure is constant. The results presented here are for $P = 10^5$ Pa.

2.3. Species and reactions

For temperatures between 2100 K and 12 000 K, we considered 19 species: e^-, S, S^-, S^+, S_2, S_2^+, F, F^-, F^+, F_2, F_2^+, SF, SF^-, SF^+, SF_4, SF_5, SF_6, SF_2, SF_3.

In order to avoid excessive calculation times, the minor species such as SF_5^+, SF_4^+, SF_3^+, SF_2^+, F^{2+}, S^{2+} ... were ignored. Similarly, the negative ions (F_2^-, S_2^-, SF_6^-, SF_5^- and SF_4^-), which were present in very small amounts over the temperature range considered (2100 K $< T <$ 12 000 K), were not taken into account. A preliminary study of the reactions showed that these species are only weakly involved in electron capture processes.

Sixty-six chemical reactions were taken into account and have been described in [21]. Most of the direct reaction rates proceed from [19], whereas the reverse rates were computed by microreversibility requiring the calculation of the partition functions. Details of the reactions are given in tables 1(*a*)–(*e*).

Table 1. (*b*) Chemical reaction scheme, rate determined by Arrhenius fit: $K_d = aT^B \exp(-C/T)$.

No	Chemical reaction	Ref.	*A*	*B*	*C*
3	$F + F + F \leftrightarrow F_2 + F$	[19]	5.40E-35	0	0
4	$F + S + F \leftrightarrow SF + F$	[19]	2.80E-34	0	0
5	$S + S + F \leftrightarrow S_2 + F$	[19]	4.50E-34	0	7340
6	$SF_4 + F_2 \leftrightarrow SF_6$		2.63E-11	0	7340
7	$F_2 \leftrightarrow F + F$	[21]	3.52E-11	0	16 970
8	$SF_5 + F_2 \leftrightarrow SF_6 + F$	[21]	2.63E-11	0	2438
9	$S_2 \leftrightarrow S + S$	[21]	7.95E-11	0	38 749
10	$SF_4 + F \leftrightarrow SF_3 + F_2$	[21]	6.61E-14	0	1005
11	$SF_4 + F_2 \leftrightarrow SF_5 + F$	[21]	2.63E-11	0	7340
12	$SF_4 + F \leftrightarrow SF_5$	[21]	6.61E-14	0	1307
13	$SF_5 + F \leftrightarrow SF_6$	[21]	1.66E-11	0	0
14	$SF_5 + SF_5 \leftrightarrow SF_4 + SF_6$	[21]	1.66E-11	0	854
15	$S^- + SF \leftrightarrow S + SF^-$	[29]	3.28E-11	0.5	0
16	$S^+ + S_2 \leftrightarrow S_2^+ + S$	[19]	1.38E-09	0	0
17	$S^+ + SF \leftrightarrow SF^+ + S$	[19]	1.00E-10	0	0
18	$F^+ + S_2 \leftrightarrow S_2^+ + F$	[19]	1.66E-09	0	0
19	$F^+ + SF \leftrightarrow SF^+ + F$	[19]	1.30E-09	0	0
20	$F^+ + F_2 \leftrightarrow F_2^+ + F$	[19]	6.90E-10	0	0
21	$F + e + F \leftrightarrow F^- + F(\leftarrow)$	[19]	1.00E-11	0	40 000
22	$S + e + F \leftrightarrow S^- + F(\leftarrow)$	[19]	4.23E-12	0.5	24 105
23	$SF^+ + e \leftrightarrow S + F$	[19]	3.46E-6	−0.5	0
24	$S_2^+ + e \leftrightarrow S + S$	[19]	3.46E-6	−0.5	0
25	$F_2^+ + e \leftrightarrow F + F$	[19]	3.46E-6	−0.5	0
26	$F_2 + e \leftrightarrow F + F + e$		3.00E-10	0	0
27	$S^+ + S^- + F \leftrightarrow S_2 + F$	[30]	6.32E-20	−2.5	0
28	$F^- + S^+ + F \leftrightarrow SF + F$	[30]	7.32E-20	−2.5	0
29	$S + S^+ + F \leftrightarrow S_2^+ + F(\leftarrow)$	[19]	3.81E-12	0.5	74 735
30	$F + S^+ + F \leftrightarrow SF^+ + F(\leftarrow)$	[19]	3.92E-12	0.5	43 750
31	$S + F^- + F \leftrightarrow SF^- + F(\leftarrow)$	[19]	3.92E-12	0.5	24 950
32	$F + S^- + F \leftrightarrow SF^- + F(\leftarrow)$	[19]	3.92E-12	0.5	40 849
33	$S_2^+ + F^- + F \leftrightarrow S_2 + F + F$	[30]	6.61E-20	−2.5	0
34	$S_2^+ + F^- + F \leftrightarrow SF + F + S$	[30]	6.61E-20	−2.5	0
35	$S_2^+ + F^- + F \leftrightarrow S_2 + F_2$	[30]	6.61E-20	−2.5	0
36	$S_2^+ + F^- + F \leftrightarrow SF + SF$	[30]	6.61E-20	−2.5	0
37	$S^+ + SF \leftrightarrow S_2^+ + F$	[21]	9.90E-10	0	0
38	$S^+ + F_2 \leftrightarrow SF^+ + F$	[21]	5.89E-10	0	0
39	$F_2^+ + F^- \leftrightarrow F + F + F$	[31]	1.5E-07	0	0
40	$F^+ + S + F \leftrightarrow SF^+ + F(\leftarrow)$		3.91E-12	0.5	44 098
41	$F^+ + F^- + F \leftrightarrow F_2 + F$	[31]	8.18E-20	−2.5	0
42	$F^+ + S^- + F \leftrightarrow SF + F$	[30]	7.30E-20	−2.5	0
43	$F + F^+ + F \leftrightarrow F_2^+ + F(\leftarrow)$		4.09E-12	0.5	37 019

Table 1. (*c*) Chemical reaction scheme, rate determined by the Lennard–Jones method: $K_d = A\exp(B + CT + DT^2)\exp(-E/T)$.

No	Chemical reaction	Ref.	*A*	*B*	*C*	*D*	*E*
44	$SF_6 + SF_2 \leftrightarrow SF_4 + SF_4$	[21]	5.22E-20	16.669	1.25E-04	−8.10E-09	15 080
45	$SF + SF \leftrightarrow F_2 + S_2$	[21]	5.22E-18	16.549	1.03E-04	−5.72E-09	12 470
46	$F + SF \leftrightarrow F_2 + S$	[21]	5.22E-18	16.347	1.50E-04	−1.07E-08	22 270
47	$F + SF \leftrightarrow SF_2$	[21]	5.22E-18	16.347	1.50E-04	−1.07E-08	0
48	$F_2 + S \leftrightarrow SF_2$	[21]	5.22E-19	16.572	9.99E-05	−5.34E-09	5027
49	$SF + F_2 \leftrightarrow SF_2 + F$	[21]	5.22E-19	16.345	1.47E-04	−1.05E-08	5027
50	$SF + SF \leftrightarrow S + SF_2$	[21]	5.22E-18	16.549	1.03E-04	−5.72E-09	0
51	$S_2 + F_2 \leftrightarrow SF_2 + S$	[21]	5.22E-20	16.654	9.99E-05	−5.34E-09	15 080
52	$SF_2 + F \leftrightarrow SF_3$	[21]	5.22E-19	16.473	1.50E-04	−1.07E-08	5027
53	$SF_2 + F_2 \leftrightarrow SF_3 + F$	[21]	5.22E-20	16.432	1.47E-04	−1.05E-08	15 080
54	$SF + F_2 \leftrightarrow SF_3$	[21]	5.22E-19	16.345	1.47E-04	−1.05E-08	5027
55	$SF_2 + SF_2 \leftrightarrow SF_3 + SF$	[21]	5.22E-20	16.669	1.03E-04	−5.71E-09	27 420
56	$SF_3 + F \leftrightarrow SF_4$	[21]	5.22E-18	16.567	1.44E-04	−1.01E-08	0
57	$SF_2 + F_2 \leftrightarrow SF_4$	[21]	5.22E-20	16.432	1.47E-04	−1.05E-08	15 080
58	$SF_3 + SF_3 \leftrightarrow SF_2 + SF_4$	[21]	5.22E-18	16.489	1.44E-04	−1.01E-08	0
59	$SF_2 + SF_2 \leftrightarrow SF_4 + S$	[21]	5.22E-20	16.669	1.03E-04	−5.71E-09	27 960
60	$SF_3 + F_2 \leftrightarrow SF_5$	[21]	5.22E-19	16.488	1.44E-04	−1.01E-08	5027

Table 1. (*d*) Chemical reaction scheme, other rate: $K_d = A + BT + CT^2 + DT^3 + ET^4$.

No	Chemical reaction	Ref.	*A*	*B*	*C*	*D*	*E*
61	$F_2 + e \leftrightarrow F^- + F$	[32]	1.02E-08	−4.98E-13	−3.25E-16	4.67E-20	0
62	$SF + e \leftrightarrow F^- + F$	[21]					
63	$F + e + e \leftrightarrow F^- + e$	[33]	5.32E-31	−1.15E-34	1.27E-38	−6.70E-43	1.37E-47
64	$F + F \rightarrow F_2 + h\nu$		−2.87E-23	9.69E-26	−2.38E-31	9.86E-33	−5.64E-37
65	$F + e \rightarrow F^- + h\nu$	[34]	2.53E-15	−3.46E-19	3.82E-23	−1.86E-27	3.37E-32
66	$S + e \rightarrow S^- + h\nu$	[35]	8.93E-15	−1.52E-18	1.51E-22	−5.30E-27	0

Table 1. (*e*) Unit of the constant *A* used in tables 1(*a*) to 1(*d*).

Chemical reaction	Reaction rate	Unit of *A* used in the tables
$\alpha_1 + \alpha_2 + \alpha_3 + \cdots + \alpha_j \rightarrow \beta_1 + \beta_2 + \beta_3 + \cdots + \beta_l$	K_d	$cm^{3(j-l)}\ s^{-1}$

2.4. Equations

The conservation equation for species i is given by

$$\frac{\partial n_i}{\partial t} + \nabla \cdot (\boldsymbol{n}_i \boldsymbol{V}) = Ca_i - n_i Da_i. \tag{1}$$

The terms Ca_i and Da_i describe the chemical reaction rates and were calculated previously [20, 21]. In equilibrium conditions, the creation term is equal to the loss term and the SF_6 plasma composition is calculated by equation (1) which comes down to

$$n_i = \frac{Ca_i}{Da_i}. \tag{2}$$

The model is composed of 19 reaction rate equations. In fact these equations (2), written for the stationary state, are not linearly independent. Other relations exist to link the particle densities: the perfect gas law, electrical neutrality and stoichiometric equilibrium between S and F in the plasma. We thus obtained a table of plasma densities for temperatures between 12 000 K and 2100 K with a step of 50 K.

2.5. Results

Calculation gives the equilibrium composition which may be used to analyse the results of the kinetic model and to estimate the relaxation times (also called reaction time constants). As an example, figure 1 shows the variations of the equilibrium particle densities versus temperature at atmospheric pressure (10^5 Pa). Between 12 000 K and 4500 K, the electrons and the S^+ ions constitute the majority of the charged species.

Below 4500 K and down to 2500 K, S_2^+ and F^- are the major ions. It can be noted that the diatomic species SF and S_2 are more abundant than F_2 at temperatures between 3500 K and 6000 K. In order to validate our kinetic model, we compared the composition obtained with that calculated using a thermodynamic model [4]. We found a good agreement between the two series of results and with the results in the literature [19].

3. Kinetic estimates

This section reports a study of the chemical kinetics of SF_6. During arc decay, strong blowing occurs and the column of plasma can be locally cut by a layer of cold gas with a very low electrical conductivity preventing the electric current from circulating. The input of this cold gas in the hot regions of the plasma tends to cause the disappearance of electrons. In this study we investigate the molecular species (SF_X ($X = 2$–6), S_2, SF and F_2) which, under the influence of convection, can reach the hot zones. We will look at the species that favour electron disappearance and the dominant reactions involved.

The general chemical reaction of dissociation or recombination between atoms and molecules is given by relation (3), where K_d represents the direct rate and K_i the reverse rate. At equilibrium, the rate of direct reactions is equal to the rate of reverse reactions per unit time and volume (4).

Considering reaction 'p':

$$\mathrm{A} + \mathrm{B} \underset{K_i}{\overset{K_d}{\rightleftarrows}} \mathrm{C} + \mathrm{D} \tag{3}$$

$$n_\mathrm{A} n_\mathrm{B} K_d = n_\mathrm{C} n_\mathrm{D} K_i. \tag{4}$$

The relaxation time τ_p^A of species A for this reaction 'p' is a function of the reaction rate K_d and of the density n_B and is given by

$$\tau_p^\mathrm{A} = (K_d n_\mathrm{B})^{-1} \tag{5}$$

and the total relaxation time of the species A for N reactions is (N is the total number of chemical reactions where A species is involved) is

$$\frac{1}{\tau^\mathrm{A}} = \sum_{p=1}^{N} \frac{1}{\tau_p^\mathrm{A}}. \tag{6}$$

In order to see if the electron number density can decrease by recombination, we studied the relaxation time associated with the species. For a given velocity v of particle 'i' we

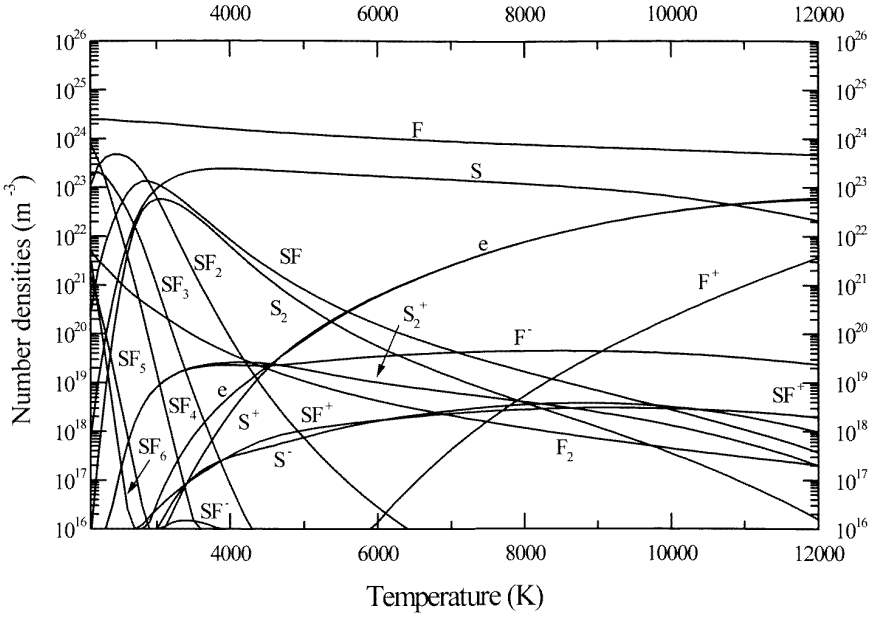

Figure 1. Variations of densities in SF_6 plasma equilibrium.

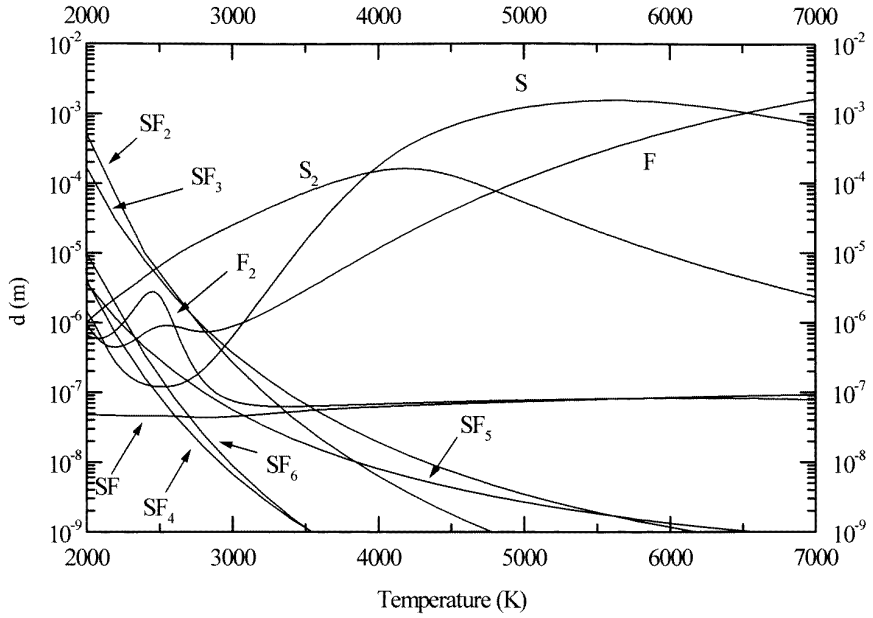

Figure 2. Mean path of molecules before dissociation in the plasma.

can define 'd' as the mean length or distance that the species can travel before being dissociated

$$d = v\tau^{\mathrm{A}} \tag{7}$$

where τ^{A} is the relaxation time, giving the time characteristic necessary to return to the equilibrium value of the density. With an arbitrary value of the velocity, 'd' gives an idea of the possibilities of the molecules arriving in the hot regions.

The mean length 'd' is presented in figure 2 versus the temperature for a velocity of 10 m s^{-1} for polyatomic species SF_X (X = 2–6), diatomic species (S_2, SF, F_2) and atomic species (S, F). For the polyatomic species, an increase of the temperature leads to a decrease of 'd'. At 2500 K, the value of 'd' is between 10^{-8} m and 10^{-7} m, indicating very fast dissociation of these species. Figure 2 shows that SF_X (X = 2–6) molecules have a low probability of penetrating hot regions ($T > 3000$ K). The relaxation length d is calculated using a low velocity of 10 m s^{-1}; in real circuit breakers the velocities are much greater than that considered here, so the order of magnitude obtained here for the relaxation length must be weighted

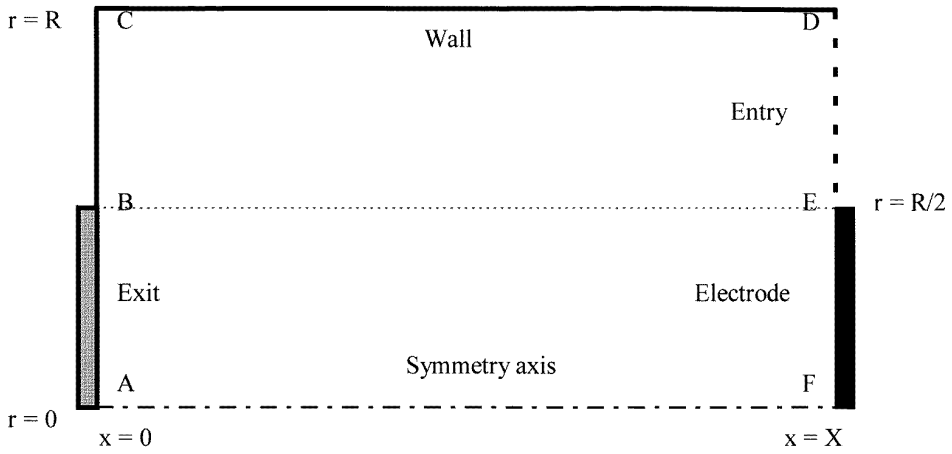

Figure 3. Calculation domain and boundary conditions.

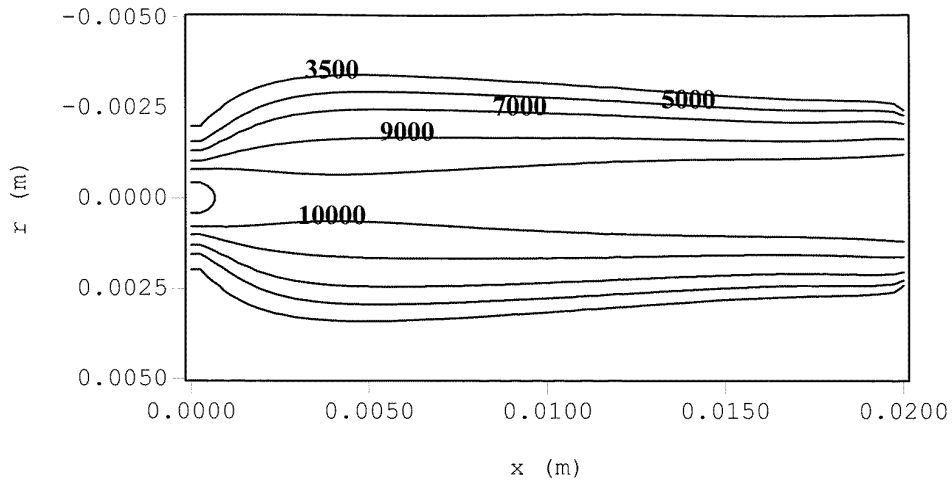

Figure 4. Plasma temperature field (t = 0 μs) (K).

by the real velocity. The distance 'd' for diatomic species, which is more stable at high temperatures, is greater than that for polyatomic molecules. The atomic species present greater values, indicating a low dissociation of the species, but with regard to the temperature range 4000 K to 6000 K the reactions show that the electronic attachment is not important. There are two consequences of this result: first, the effect of convection on the electron density could occur through the diatomic molecules (S_2). Secondly, the polyatomic molecule densities should have values near the equilibrium composition.

4. Hydrokinetic model

4.1. Hypothesis of the model

The model deals with a 2D SF_6 arc in the transient state and limited by a cylindrical wall. It is based on the following main assumptions: the plasma has a cylindrical symmetry and is in thermal equilibrium (locally we define only one temperature $T = T_e = T_h$); we consider that the transport coefficients (electrical conductivity σ, thermal conductivity κ, specific heat C_P, viscosity μ [4], net emission coefficient ε_N [26]) are only dependent on temperature and pressure. The net emission coefficient has been used, assuming a mean plasma radius of 2 mm. Diffusion of particles is ignored. Without an electric field, the electron diffusion velocity term $\langle v_e \rangle$ can be estimated using the relation

$$n_e \langle v_e \rangle \approx -D_a \nabla(n_e). \tag{8}$$

For ambipolar diffusion, the electron diffusion velocity is equal to the ion diffusion velocity. The equilibrium plasma composition shows that S^+ density is very close to the electron density. Fluorine atoms correspond to the majority atomic species so the ambipolar diffusion coefficient can be written as

$$D_a \approx 2D_{S^+F}. \tag{9}$$

We have not found any literature values for the diffusion coefficient D_{S^+F}, but unpublished work by Gleizes and Razafinimanana has estimated this coefficient to be equal to 7 cm^2 s^{-1} for a temperature equal to 6000 K. This value is very closed to the value obtained in an argon plasma at the same temperature. So the diffusion velocity can

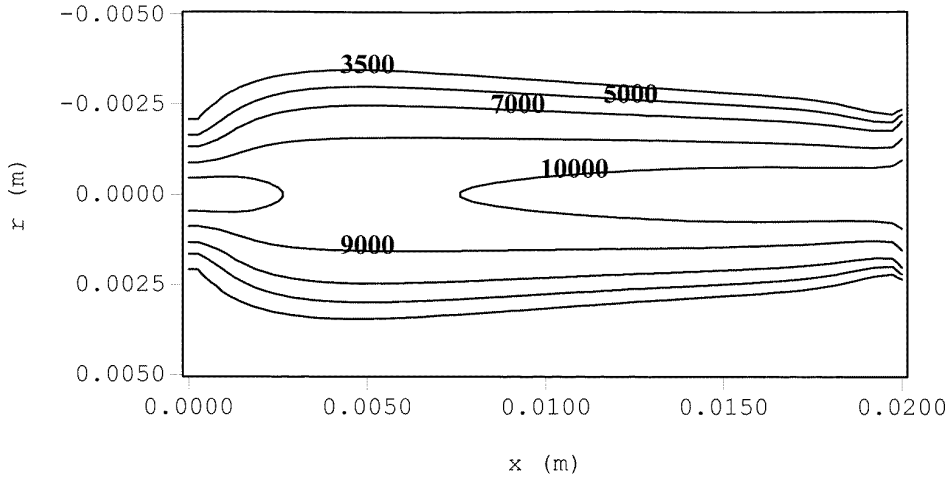

Figure 5. Plasma temperature field (t = 5 μs) (K).

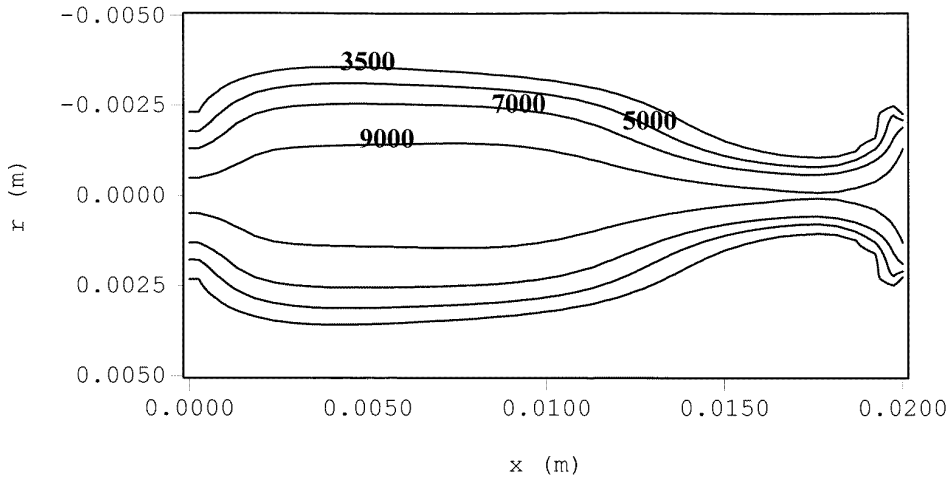

Figure 6. Plasma temperature field (t = 15 μs) (K).

be estimated, and the maximum value of the diffusion velocity can be estimated as 10 m s^{-1} for a radial convection velocity equal to 60 m s^{-1}. In the others cases the ambipolar diffusion velocity is at least an order of magnitude lower than the radial convection velocity.

4.2. Calculation domain and boundary conditions

The calculation domain and boundary conditions are given in figure 3 and table 2. The dimensions of the calculation domain are 2 cm and 0.5 cm in the axial and radial directions respectively for a grid of 40×40 points. On the electrode (line EF) we made a preliminary study, resolving the 1D energy equation (see equation (19) later) in the stationary state in order to find the boundary conditions for the resolution of the 2D stationary model.

The region in figure 1 between 2100 and 3000 K corresponds to a transition zone where diatomic species recombine to form polyatomic species. During this abrupt alteration of the population from one of diatomic species to one of polyatomic species, numerical instability can occur in our model. To overcome this problem, we set the temperature at the wall (line BCD) at 3000 K. Assuming the wall temperature equal to 3000 K leads only to an underestimation of the plasma cooling. Indeed for temperatures lower than 3000 K the thermal conductivity presents peaks corresponding to the dissociation of SF_6, SF_4 and SF_2, and these peaks are not taken into account. In our study, the wall temperature has little influence on the calculation of the electron number density. At 3000 K the electron density is very low; moreover, the study reported in section 3 shows that deviations from the equilibrium composition up to 3000 K are very weak owing to the very short relaxation times of the polyatomic species.

In the stationary state, gas entry is situated on line DE where the axial velocity profile $u(r)$ of the inlet flow is assumed to be parabolic

$$D_0 = 2\pi \int_{R/2}^{R} \rho u r \, \mathrm{d}r. \tag{10}$$

The mass flow rate D_0 is equal to 0.2 g s^{-1}. In order to limit the axis temperature in the stationary state (the

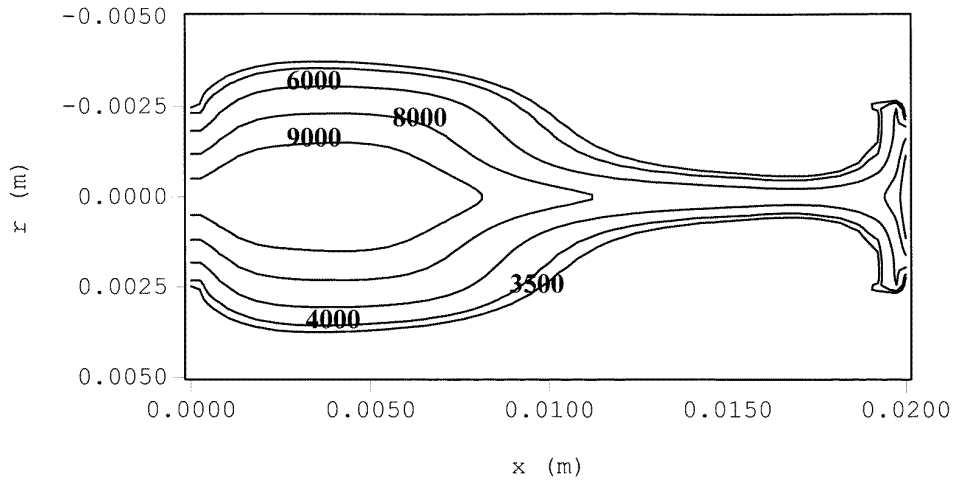

Figure 7. Plasma temperature field (t = 20 μs) (K).

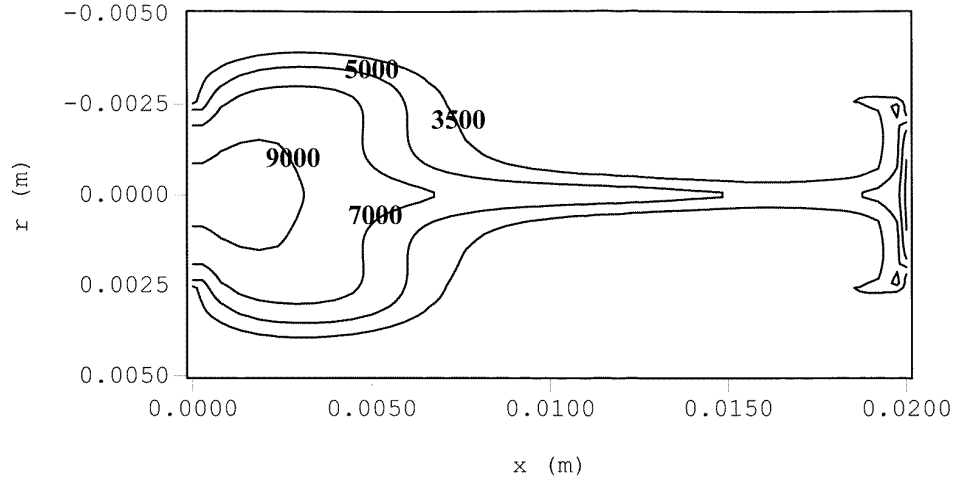

Figure 8. Plasma temperature field (t = 25 μs) (K).

Table 2. Boundary conditions for the hydrokinetics model.

	AB	BCD	DE	EF	FA
u	$\partial u/\partial x = 0$	0	$u(r, t)$	0	$\partial u/\partial r = 0$
v	0	0	0	0	0
T	$\partial T/\partial x = 0$	3000 K	3000 K	$\partial T/\partial x = 0$	$\partial T/\partial r = 0$
n	$\partial n/\partial x = 0$	$\partial n/\partial r = 0$	n_{LTE}	n_{LTE}	$\partial n/\partial r = 0$
P	$\partial P/\partial x = 0$	$\partial P/\partial r = 0$	P_0 = 0.1 MPa	P_0 = 0.1 MPa	$\partial P/\partial r = 0$

reaction rates were computed for $T \leq 12\,000$ K) and to have rather strong blowing during extinction, we imposed an increasing inlet flow in the transient state given by (9), during the first 20 μs

$$D(t) = D_0\left(1 + \frac{29t}{2 \times 10^{-5}}\right) \qquad (0 < t < 2 \times 10^{-5}\ \mathrm{s}) \tag{11}$$

$$D(t) = 30D_0 \qquad (t > 2 \times 10^{-5}\ \mathrm{s}).$$

We will now give the conservation equations for stationary and transient states. The resolution of these equations is based on the algorithms of Patankar [27]. The boundary conditions on the pressure are directly deduced from the density conditions, so we have at the entry (DE) an inlet given pressure $P = 0.1$ MPa and Neumann conditions on BCD and AB. The pressure variations are weak during the arc decay; results in the pressure field are presented in section 4.5.

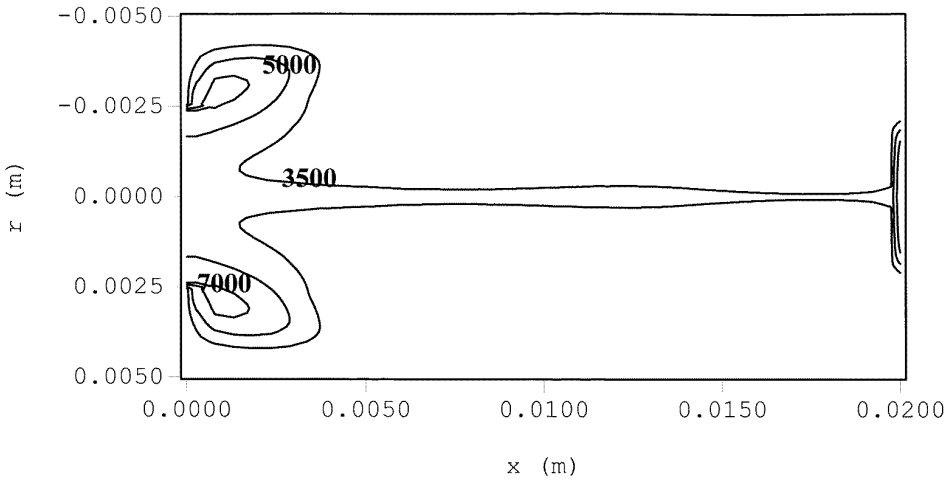

Figure 9. Plasma temperature field (t = 40 μs) (K).

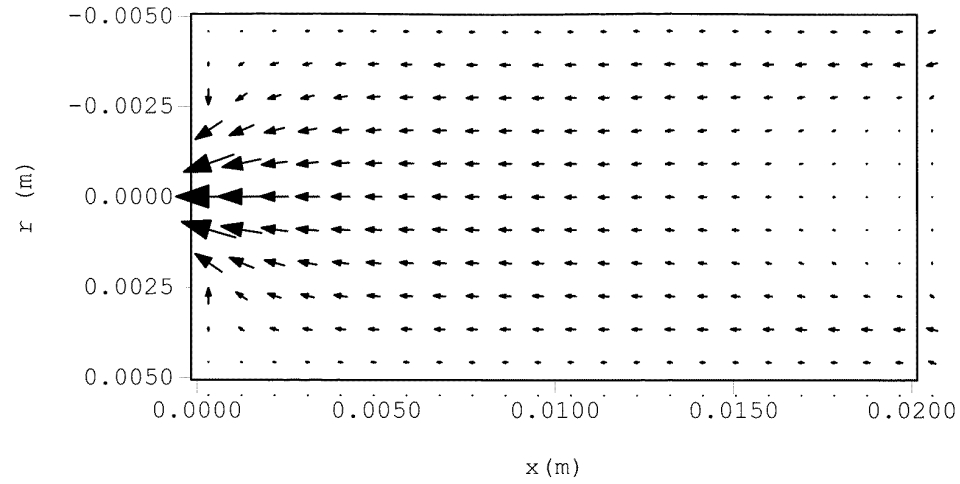

Figure 10. Velocity field (t = 0 μs) (m s^{-1}).

4.3. Equations

The parameters to be calculated (temperature, velocity and pressure) depend on the local variables r (radial distance) and x (axial distance). In the transient state we also calculate the species densities; all the unknowns are then dependent on the three variables (space and time).

(i) *Mass conservation:*

$$\frac{\partial}{\partial x}(\rho u) + \frac{1}{r}\frac{\partial}{\partial r}(r\rho v) = 0. \tag{12}$$

The mass conservation (12) is only used in the stationary state: in the transient state the mass conservation is satisfied indirectly by assuming the species conservation (equation (1)).

(ii) *Axial momentum:*

$$\rho\frac{\partial u}{\partial t} + \rho u\frac{\partial u}{\partial x} + \rho v\frac{\partial u}{\partial r} = -\frac{\partial P}{\partial x} + 2\frac{\partial}{\partial x}\left(\mu\frac{\partial u}{\partial x}\right) + \frac{1}{r}\frac{\partial}{\partial r}\left(r\mu\frac{\partial u}{\partial r}\right) + \frac{1}{r}\frac{\partial}{\partial r}\left(r\mu\frac{\partial v}{\partial x}\right). \tag{13}$$

(iii) *Radial momentum:*

$$\rho\frac{\partial v}{\partial t} + \rho u\frac{\partial v}{\partial x} + \rho v\frac{\partial v}{\partial r} = -\frac{\partial P}{\partial r} + \frac{\partial}{\partial x}\left(\mu\frac{\partial v}{\partial x}\right) + \frac{2}{r}\frac{\partial}{\partial r}\left(r\mu\frac{\partial v}{\partial r}\right) + \frac{\partial}{\partial x}\left(\mu\frac{\partial u}{\partial x}\right) - \frac{2\mu v}{r^2} - J_x B_\theta. \tag{14}$$

In the transient state the last term is equal to zero.

(iv) *Energy conservation:*

$$\rho\frac{\partial h}{\partial t} + \rho u\frac{\partial h}{\partial x} + \rho v\frac{\partial h}{\partial r} = +\frac{\partial}{\partial x}\left(\Gamma\frac{\partial h}{\partial x}\right) + \frac{1}{r}\frac{\partial}{\partial r}\left(r\Gamma\frac{\partial h}{\partial r}\right) + \sigma E^2 - 4\pi\varepsilon_N + u\frac{\partial P}{\partial x} + v\frac{\partial P}{\partial r} \tag{15}$$

with $\Gamma = \kappa/C_P$. In the transient state, the electric field is set to zero.

(v) *Ohm's law:*

$$E = E_x = \frac{I}{G} \tag{16}$$

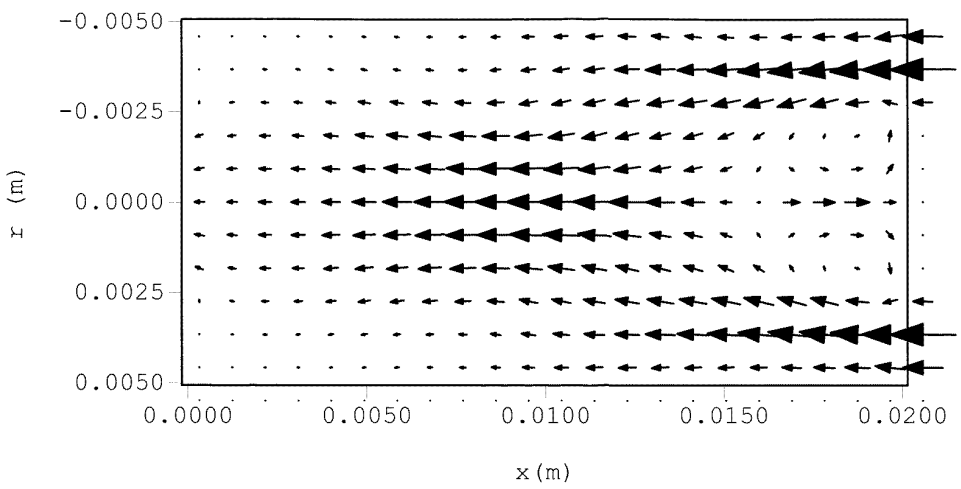

Figure 11. Velocity field (t = 20 μs) (m s^{-1}).

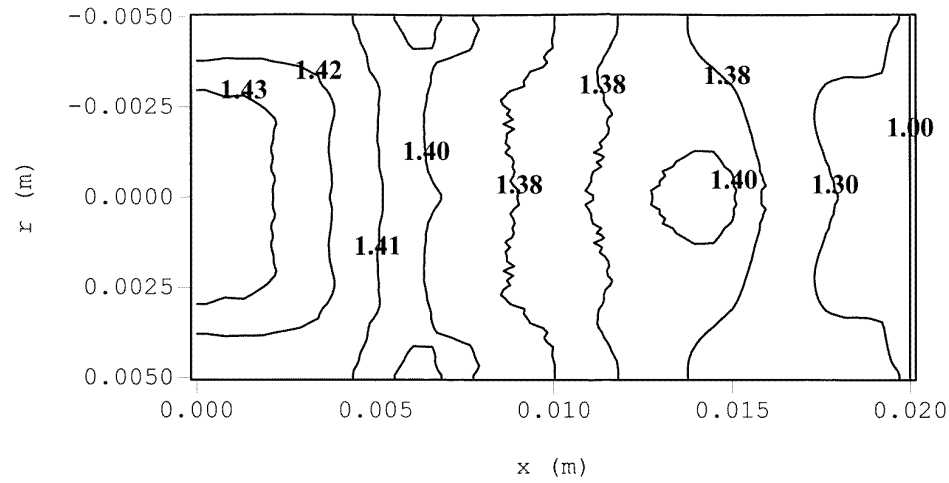

Figure 12. Pressure field (t = 20 μs).

$$G = 2\pi \int_0^R \sigma r \, \mathrm{d}r \tag{17}$$

(vi) *Maxwell–Ampere law:*

$$B_\theta = \frac{\mu_0}{r} \int_0^r j_x \xi \, \mathrm{d}\xi. \tag{18}$$

(vii) *Energy equation near the electrode:*

$$\frac{1}{r}\frac{\partial}{\partial r}\left(r\kappa \frac{\partial T}{\partial r}\right) + \sigma E^2 - 4\pi\varepsilon_N = 0. \tag{19}$$

(viii) *Coupling equations:*

(a) perfect gas law: $P = \sum_i n_i k_b T$ (20)

(b) mass density: $\rho = \sum_i m_i n_i$. (21)

4.4. Calculation

In the stationary state the calculation is made for a current intensity I of 50 A, the electric field E being constant and uniform. The calculation procedure starts by resolving the energy equation (19). Resolution of this equation allows boundary conditions to be set for the temperature on the surface of the upstream electrode. Equation (19) is resolved by setting a temperature of 3000 K at the edges of the electrode (point E). This corresponds to the temperature of the gas at the inlet (DE) and that of the walls. The temperature profile determined for $x = 0$ on section EF is then used to initialize the calculation range. The model is then resolved in two dimensions to obtain the stationary solution.

Initialization with this method enables the calculation to be started off as stable. On extinction, from $t = 0$, the electric field is taken as being nil. The initial profiles of temperature and velocity are given by the stationary model and the initial densities of the 19 species are given by the equilibrium composition. The models (hydrodynamic and

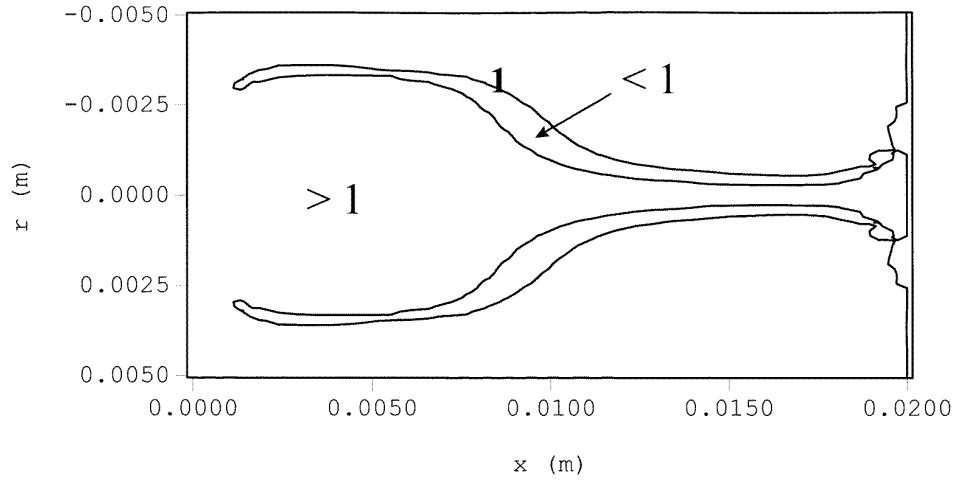

Figure 13. Relative density field (electron, t = 20 μs).

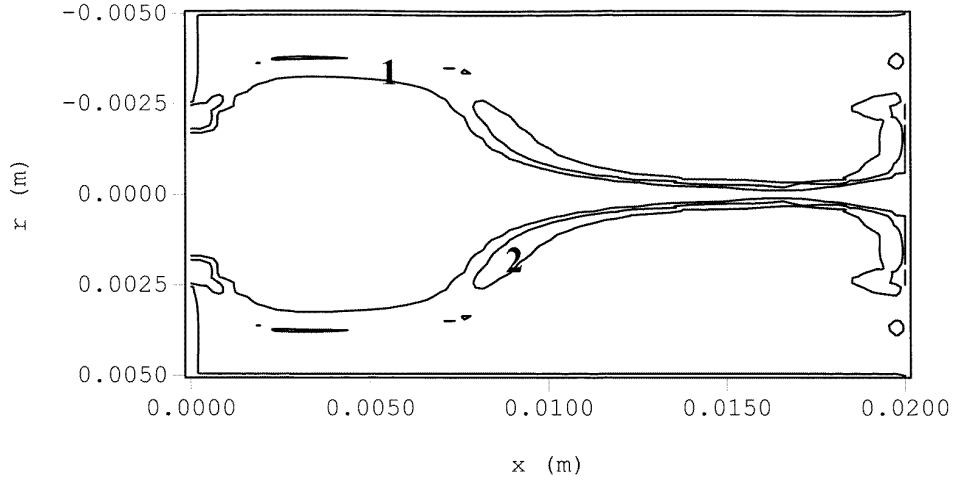

Figure 14. Relative density field (S_2^+, t = 20 μs).

kinetic) are linked through pressure (20) and mass density (21). The time step Δt is set at 10^{-10} s; this value is chosen using a kinetic criterion, $\Delta t = [(Da)_{\max}]^{-1}$, were $(Da)_{\max}$ represents the maximum value of Da_i. For the calculation of time Δt, the densities of the molecular SF_X ($X = 2$–6) species are not taken into account.

4.5. Results

We shall present a few results of the hydrokinetic model during arc decay for an initial pressure of one atmosphere. The kinetic values, the reaction rates, the partition functions and the initial densities are collected for temperatures up to 12 000 K. In order for this boundary value not to be exceeded in our calculation, the initial temperature was calculated by setting the initial stationary current at 50 A.

In figures 4 to 9, we present the temperature fields (in K) during decay for times of 0, 5, 15, 20, 25 and 40 μs respectively. For the initial instant and 20 μs figures 10 and 11 report the corresponding velocity fields (in m s^{-1}). At the initial instant, it can be seen that the temperature maximum is located at the outlet of the discharge for a maximum outlet velocity of 335 m s^{-1} (figure 10). Indeed, the input gas is injected in a ring with an axial velocity component. It therefore only penetrates very slightly into the heart of the plasma. The gas outlet, however, is located at the centre of the discharge and has a cross-sectional area which is smaller than the inlet. The radial velocities therefore increase towards the outlet causing confinement of the plasma and an increase in temperature.

Figures 5 to 8 show that a constriction occurs on the temperature profiles near the upstream electrode. On extinction there is an increase of the radial velocities towards the axis of the arc because of pumping phenomena which tend to compensate for the drop in pressure caused by cooling. We then see the steady inclusion of the cold injection gas which disturbs the plasma by cooling it. This is illustrated in figure 11 where the velocities can be seen to steadily reach the core of the plasma, come up against its high viscosity and form eddy currents. At 20 μs, the Mach

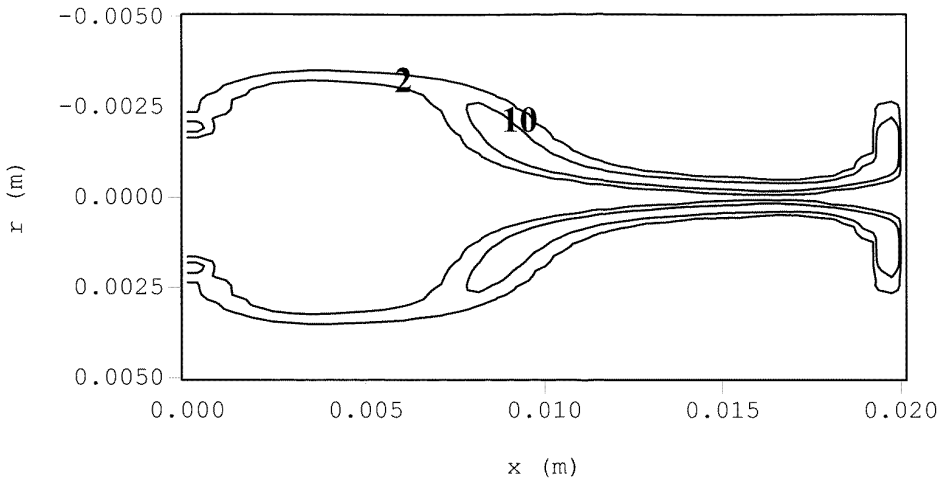

Figure 15. Relative density field (S_2, t = 20 μs).

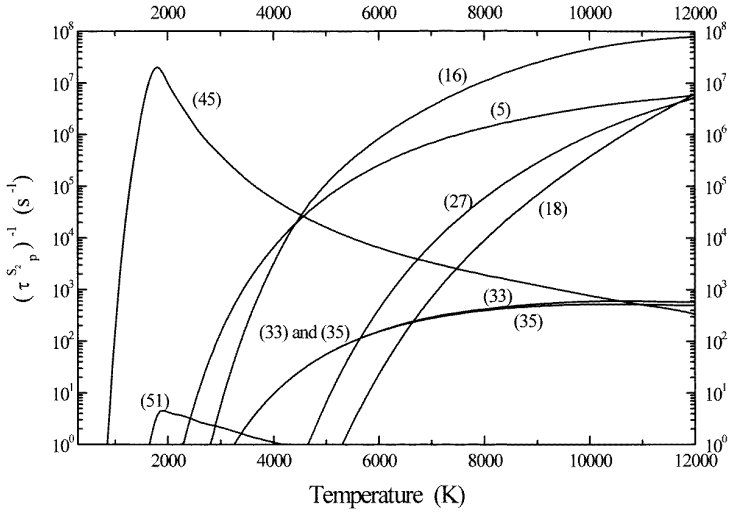

Figure 16. Contribution of the reactions to the inverse total relaxation time of the species S_2.

number is close to 1 everywhere, with maximum values of 1.4 on the input layer (line DE). At 40 μs, the temperature field in figure 9 shows that the arc is almost extinguished.

Figure 12 represents the pressure field over the whole calculation range, at $t = 20$ μs. The input pressure is fixed at one atmosphere. The steady increase of the flow imposed at the inlet and the low surface area of the outlet lead to excess pressure: the gas enters the chamber at relatively low temperature (3000 K) but, owing to the high local temperatures at the outlet (figure 7), where the mass densities are lower, there is an accumulation of gas. The boundary conditions set for the species densities lead to the outlet pressure not being fixed.

In figure 13 we have plotted the relative electron number density field (the relative density is defined as the ratio of the calculated number density to the equilibrium value of the local pressure and temperature). Our results mainly show an underpopulation of electron density at the edges of the plasma, i.e. in the temperature range 4000 K $<$ T $<$ 6000 K. In figures 14 and 15 we have plotted the relative densities of S_2^+ and S_2 respectively. We can note an overpopulation of S_2^+ and S_2 at the edges of the arc. The underpopulation of electron density is explained by electron recombination with S_2^+ molecules, this effect being enhanced by cold gas convection. In fact, it is difficult to compare the results obtained with two different values of the inlet mass flow rate. For a given time, the temperature fields are not identical, but a comparison made between two different times leading to approximately the same temperature field shows that the electron underpopulation is accentuated by the convection. In figures 16, 17 and 18 we have plotted the inverse partial relaxation times of species S_2, S_2^+ and electrons respectively versus the temperature for various chemical reactions. Figure 16 shows that charge exchange (reaction 16, see table 1(b)) $S^+ + S_2 \leftrightarrow S + S_2^+$ is responsible for the creation of the molecule S_2^+ when T $>$ 4000 K. Indeed, equation (6) shows that for high values of τ_A^{-1} there is strong disappearance of S_2 (reaction

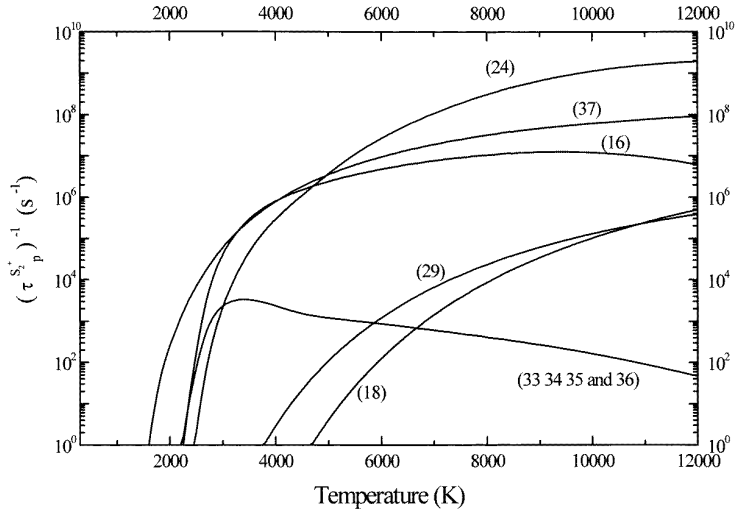

Figure 17. Contribution of the reactions to the inverse total relaxation time of the species S_2^+.

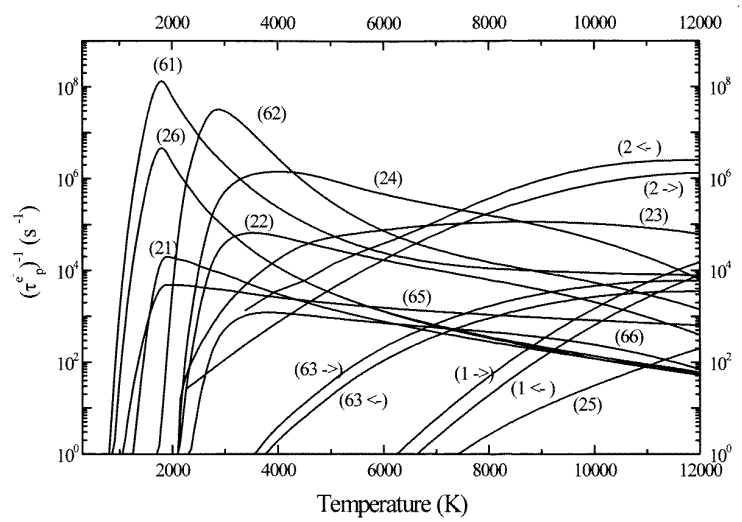

Figure 18. Contribution of the reactions to the inverse total relaxation time of the electron.

16) and therefore abundant formation of S_2^+. Figures 17 and 18 show that electron–ion recombination (reaction 24) $S_2^+ + e \leftrightarrow S + S$ is responsible for the disappearance of electrons in the temperature range 4000 K to 6000 K.

The results show that departures from equilibrium created by strong convection can lead to an increase in the plasma resistivity. They show a disappearance of the electron density more quickly than we can deduced from an equilibrium composition in the temperature range 4000–6000 K. But as we found using the equilibrium model, it is a critical temperature range for thermal cut-off in SF_6 circuit breakers.

5. Conclusion

In this paper we first presented a study of the chemical kinetics of SF_6, then we presented a hydrokinetic model. The kinetic study brought out the following points: from the study of the reaction rates, we showed that polyatomic molecules cannot penetrate into the hot regions containing the electrons. However, the penetration of S_2 molecules leads to an overpopulation of S_2^+ which traps electrons.

The hydrodynamic model, using simplified geometry, predicts the occurrence of electron underpopulation in regions where the temperature is between 4000 and 6000 K, a critical temperature range for thermal cut-off in SF_6 circuit breakers. The study has shown that the disappearance of electrons can be explained by electron–ion recombination with S_2^+ molecules and that this effect is enhanced by cold gas convection.

This paper is the first step in the study of deviations from equilibrium in models of decaying circuit-breaker arcs. Now we are developing a two-temperature model that may include deviations from thermal equilibrium occurring when a recovery voltage is applied to the decaying arc plasma.

Acknowledgments

This work was partly financed by a contract with Electricité de France (EDF) and GEC-Alsthom.

References

[1] Hermann W, Kogelschatz U, Niemeyer L, Ragaller K and Shade E 1974 *J. Phys. D: Appl. Phys.* **7** 607
[2] Tuma D T and Lowke J J 1975 *J. Phys. D: Appl. Phys.* **46** 3361
[3] Cowley M D 1974 *J. Phys. D: Appl. Phys.* **7** 2218
[4] Chervy B, Gleizes A and Razafinimanana M 1994 *J. Phys. D: Appl. Phys.* **27** 1193
[5] Hermann W and Ragaller K 1977 *IEEE Trans. Power Appar. Syst.* **96** 5
[6] Tuma D T 1980 *IEEE Trans. Power Appar. Syst.* **99** 6
[7] Gleizes A, Mahieddin Rahal A, Papadopoulos S and Vacquié S 1988 *IEEE Trans. Plasma Sci.* **16** 6
[8] Gleizes A, Mitiche M and Pham Van Doan 1991 *IEEE Trans. Plasma Sci.* **19** 1
[9] Lowke J J 1992 *Bull. Tech. University Brno* **2–4** 11
[10] Fang M T C 1992 *Bull. Tech. University Brno* **2–4** 65
[11] Lowke J J, Voshall R E and Ludwig H C 1973 *J. Phys. D: Appl. Phys.* **44** 3513
[12] Gleizes A, Sakalis I, Razafinimanana M and Vacquié S 1987 *J. Phys. D: Appl. Phys.* **61** 510
[13] Gleizes A, Robert T, Gonzalez J J and Pons A 1993 *J. Phys. D: Appl. Phys.* **26** 1439–44
[14] Gonzalez J J, Gleizes A and Krenek P 1987 *J. Phys. D: Appl. Phys.* **27** 985–93
[15] Robin-Jouan P, Rathoin S, Serres E, Chevrier P, Barrauld M, Fievet Ch, Comte A, Boucher T and Vérité J C 1997 *Proc. Gas Discharges and their Applications* vol 2, ed G Babucke, p 578
[16] Chevrier P, Maftoul J and Rachard H 1997 *Proc. Gas Discharges and their Applications* vol 1, ed G Babucke, p 38
[17] Fang M T C, Zhuang Q and Guo X J 1994 *J. Phys. D: Appl. Phys.* **27** 74–83
[18] Fang M T C and Zhuang Q 1992 *J. Phys. D: Appl. Phys.* **25** 191–204
[19] Brand K P and Kopainsky J 1978 *Appl. Phys.* **16** 245
[20] Gleizes A, Mbolidi F, Razafinimanana M, Vacquié S and Gravelle D 1991 *J. Phys. D: Appl. Phys.* **24** 1333–8
[21] Borge E 1995 *Doctoral thesis* University Paul Sabatier, Toulouse
[22] Adamec L 1990 *Acta Phys. Slov.* **2** 39
[23] Adamec L, Bartlova M and Coufal O 1996 *Proc. XIIth Symp. on Physics of Switching Arcs* vol 1 (Brno: Department of Electrical Machines and Apparatus) **1** p 5
[24] Cliteur G J, Suzuki K, Ikeda H and Sakuta T 1997 *Proc. Gas Discharges and their Applications* vol 2, ed G Babucke, p 574
[25] Drawin H W 1979 *J. Physique Coll.* C7 **149** 40
[26] Gleizes A, Gonzalez J J, Liani B and Raynal G 1993 *J. Phys. D: Appl. Phys.* **26** 1921
[27] Patankar S V 1980 *Numerical Heat Transfer and Fluid Flow* (Washington, DC: Hemisphere)
[28] Gleizes A, Habib A A M and Vacquié S 1989 *J. Phys. D: Appl. Phys.* **22** 1464
[29] Christophorou L G 1971 *Atomic and Molecular Radiative Physics* (London: Wiley–Interscience)
[30] Drawin H W and Emard F 1975 *Beitr. Plasma Phys.* **15** 273
[31] Wilson J W and Shapiro A 1980 *J. Appl. Phys.* **51** 2387
[32] McCorkle D L, Christophorou L G, Christodoulidus A A and Pichiarella L 1986 *J. Phys. Chem.* **85** 1966
[33] Peart B, Forrest R and Dolder K T 1979 *J. Phys. B: At. Mol. Phys.* **12** L115
[34] Vacquié S, Gleizes A and Sabsabi M 1987 *Phys. Rev.* A **35** 1615
[35] Robinson E J and Geltman G 1967 *Phys. Rev.* **153** 1